Quantum Electronics **46** (4) 342–346 (2016)

DOI: 10.1070/QEL16041

Target optimisation for the yield of X-rays of desired hardness under femtosecond pulse irradiation

A.V. Brantov, M.G. Lobok, V.Yu. Bychenkov

Abstract. **Different regimes of electron acceleration from solid foils and low-density targets are investigated using three-dimensional numerical simulations. The size of the plasma corona is shown to be the main parameter characterising the temperature and number of hot electrons, which determine the yield of X-ray radiation and its hardness. Also studied is the generation of X-ray radiation by laser-accelerated electrons, which bombard the converter target located behind the laser target.**

Keywords: *femtosecond laser radiation, electron acceleration, X-ray radiation.*

1. Introduction

Bright X-ray sources with radiating spot dimensions of several micrometres are in great demand in therapy, medical diagnostics, biology, and materials science. Similar sources may also be used for the strength bench test of microchips, which is important for improving the reliability of the components of computer systems operating in space and safety systems (inspection).

Micrometre-sized sources of laser-accelerated electrons based on the interaction of high-intensity femtosecond laser pulses with different targets are perfectly suited for producing X-ray pulses either due to the electron radiation (for instance, betatron radiation) in the laser target itself or due to their conversion to continuous (bremsstrahlung) or linear (characteristic) radiation in a converter target.

X-ray sources with a moderate radiation penetration depth intended for inspecting quasi-static objects might be made using femtosecond lasers with a moderate output power to provide the generation of photons with energies of several tens of kiloelectronvolts. However, a high laser-pulse repetition rate is required in this case. Here, the greatest promise is shown by a phase contrast technique, which has already been used for obtaining microtomograms of a biological sample [1]. Of indisputable interest is the more distant prospect of generating hard (~1 MeV) radiation pulses with a brightness sufficient for producing images in one shot. The use of two-to-several of such pulses with a short (pico- and nanosecond) time delay would make it possible to study fast processes occurring deep in a dense substance and would be a diagnostic breakthrough in high energy density physics.

The development of a commercial X-ray source based on a laser with a short pulse duration encounters the problem of low conversion efficiency to X-rays, which is usually under 10^{-4} for the multikiloelectronvolt energy range and is several orders of magnitude lower for the gamma-ray range (above 100 keV). Naturally its improvement involves the quest for the most efficient targets and interaction schemes with laser pulses. Discussed in this connection are massive [2–4] and thin [5] dense solid and liquid targets, gaseous [1] and cluster [6] media, micro- and nanostructured targets [7, 8]. Another important factor involves the invention of interaction schemes that may be realised, not only theoretically but also practically, for lasers with a high pulse repetition rate.

From the standpoint of laser-plasma interaction, efficient generation of X-ray pulses invites maximising the number of accelerated electrons of prescribed energy required for the production of photons with desired energy. Studied in our work are different targets (superthin solid foil, the like semitransparent foil, a thin film of a low-density material, a dense target with a preplasma) for determining the highest-efficiency targets for the purpose specified, even if not meeting the criterion for technology reliability at this stage of investigations. Here, use is made of the same simple method of generating X-rays as in a microfocus X-ray tube, when a laser-accelerated electron beam bombards the target. For the sake of definiteness we consider the generation of hard X-ray (gamma ray) radiation in the range of hundreds of kiloelectronvolts.

2. Electron acceleration from solid and low-density targets

The main task of simulations was the search for an optimal target for generating an electron beam directed behind the target. One might expect that the use of thin foils or low-density targets would be advantageous for accelerating electrons: our previous investigations and previous investigations of other groups suggest that it is these targets that provide the formation of an efficient virtual cathode for the forward-generated electrons under the conditions of relativistic transparency. This was borne out by efficient ion acceleration behind the target [9]. The target transmittance to laser radiation is determined both by the electron density n_e [targets with a density below the relativistic critical density, $n_e < a_0 n_c$, where $n_c = \omega_0^2 m_e/(4\pi e^2)$ and $a_0 = eE/(m_e\omega_0 c)$ is the dimensionless field amplitude E for laser radiation with a wavelength $\lambda = 2\pi c/\omega_0$,

A.V. Brantov, V.Yu. Bychenkov P.N. Lebedev Physics Institute, Russian Academy of Sciences, Leninsky prosp. 53, 119991 Moscow, Russia; Centre for Fundamental and Applied Research, N.L. Dukhov All-Russia Research Institute of Automatics (VNIIA), Sushchevskaya ul. 22, 127055 Moscow, Russia; e-mail: brantov@sci.lebedev.ru;
M.G. Lobok Centre for Fundamental and Applied Research, N.L. Dukhov All-Russia Research Institute of Automatics (VNIIA), Sushchevskaya ul. 22, 127055 Moscow, Russia

Received 24 February 2016
Kvantovaya Elektronika **46** (4) 342–346 (2016)
Translated by E.N. Ragozin

are transparent to the light] and by the target thickness l (solid targets thinner than the relativistic skin layer thickness may also be transparent to light when $l \lesssim \lambda a_0 n_c/(\pi n_e)$ [10]). Below we consider both cases and compare the electron spectra produced under pulsed laser irradiation of semitransparent and opaque targets. Furthermore, a study is made of electron generation from targets with a preplasma – the plasma corona, which emerges at the front target surface, because either the laser pulse is preceded, for technical reasons, by a relatively long (multipico- or nanosecond-long) low-intensity light signal (a prepulse) or an additional weak laser pulse is intentionally employed to control the parameters of this corona.

The interaction of laser radiation with substance or plasma (depending on the importance of including ionisation) was simulated with the fully relativistic three-dimensional particle-in-cell Mandor code [11]. In our three-dimensional simulations, a linearly polarised laser pulse 30 fs in duration (with a Gaussian temporal intensity distribution) was focused to a 4-μm sized focal spot with a Gaussian radial intensity distribution on the front side of the target. The peak intensity of laser radiation was equal to 5×10^{19} W cm^{-2}, which corresponds to a laser pulse energy of 0.3 J and $a_0 = 6$ for a wavelength $\lambda = 1$ μm. In all simulations the laser pulse was incident on the target along its normal.

Initially, for a target we used a 10- or 20-nm-thick plasma layer consisting of fully ionised carbon ions and electrons. The ion density corresponded to the real solid density ($\sim$1 g cm^{-3}, which corresponded to an electron density $n_e = 200 n_c$). To study the effect of ionisation on the electron acceleration, simulations were carried out with the inclusion of ionisation of a 10-nm-thick carbon target. Next, simulations were made with the inclusion of a preplasma at the front (irradiated) side of the target. The preplasma was modelled using a linearly growing electron density, which varied from zero to the electron critical density n_c over a length of 4 to 10 μm. The thickness of the main target was equal to 20 nm. We emphasise that the target thickness is unambiguously related to the gradient of n_e for the linear density profile under consideration; in this case, the gradient length and the target thickness coincide to an order of magnitude. Additional simulations were made for a low-density plasma layer (also consisting of fully ionised carbon ions and electrons) with an electron density $n_e = 5 n_c$ and a thickness of 0.2–0.9 μm.

In our three-dimensional simulations, we employed grid steps of 0.01, 0.05, and 0.05 μm in x, y, and z axes, respectively. The laser pulse was polarised along the z axis and propagated along the x axis. The total computational domain had the following dimensions: 25 μm in the longitudinal direction and 20 μm in both transverse dimensions. The simulation time was equal to 100 fs.

The electron beam accelerated by the laser pulse is used in the second (converter) target for producing X-ray radiation. Since the second target is some distance away from the first one, it would be natural to take into account only those electrons which fly within some solid angle about the normal behind the target; the cone opening is defined by the transverse converter size and the converter separation. For definiteness, the element of cone is assumed to make an angle of 45° with the target normal (and with the direction of laser beam incidence). This ensures the delivery of all high-energy electrons to the second target if its transverse size exceeds the distance from the laser target. Therefore, recorded in our simulations was the spectrum of electrons emanating into a cone with a total opening angle of 90°.

Figure 1 serves to illustrate the effect of the target thickness on the spectra of electrons accelerated from a low-density target. We note that the number of hot electrons is little changed with target thickness variation from 0.6 to 0.2 μm, although decreasing the thickness results in an insignificant increase in the number of highest-energy electrons (with energies above 10 MeV) owing to a decrease in the number of electrons with energies of 5–10 MeV. The targets of this thickness are partially transparent to the laser radiation. The partial pulse passage through the target provides electron acceleration from the entire target volume and the efficient ejection of the highest-energy electrons behind the laser target. Increasing the target thickness (up to 0.9 μm) has the following effect: when the electrons are 'bunched up' by the ponderomotive force of the laser pulse, due to the corresponding increase in the electron density in the plasma of sufficient thickness it becomes opaque. This causes a decrease in energy and number of energetic electrons behind the target.

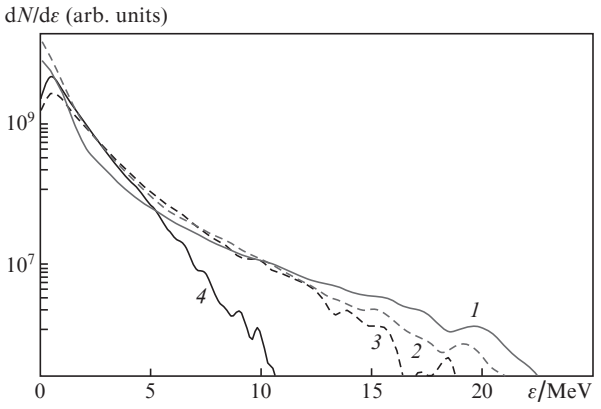

Figure 1. Spectra of the electrons emanated in a solid angle with an opening of 90° behind the target at the instant of simulation termination (t = 98 fs) in the irradiation of a low-density target ($n_e = 5n_c$) of thickness (*1*) 0.2, (*2*) 0.4, (*3*) 0.6, and (*4*) 0.9 μm.

Nonuniform plasma simulations suggest that the size of the plasma corona exerts the most significant influence on electron acceleration (Fig. 2). A nearly total reflection of the laser pulse with a perfect contrast ratio from a uniform solid target does not result in the generation of a large number of hot electrons [curve (*2*) in Fig. 2]. Decreasing the target thickness to a size which make the target semitransparent for the laser light (to 10 nm) entails some increase in the number of hot electrons. The inclusion of ionisation affects only slightly on the spectrum of hot electrons and changes it insignificantly [compare curves (*1*) and (*6*) in Fig. 2]. About the same number of electrons emanates from a low-density target with a density of the order of the relativistic critical density [curve (*3*)]. We note that it is precisely these two last-named targets (the solid semitransparent one and the target with a close-to-critical density) that are optimal for ion acceleration [9]. But electrons are most efficiently accelerated from subcritical density. That is why lowering the target density, for instance due to the emergence of a lengthy plasma corona at the target side under irradiation, entails a significant increase in the number of hot electrons. This is clearly seen in Fig. 2 [curves (*4*) and (*5*)], which shows the electron spectra for the target with a preplasma (the target itself is opaque for the laser radiation). In this case, lengthening the preplasma size increases the

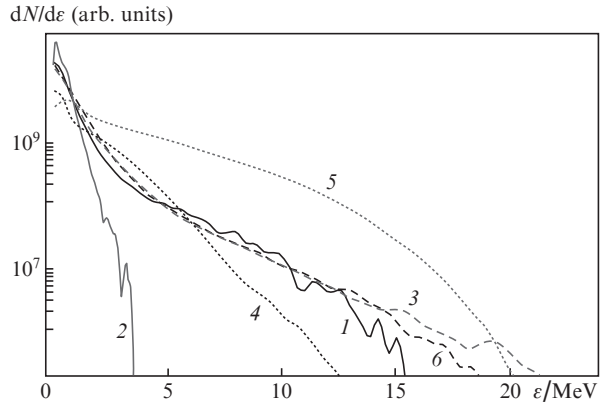

Figure 2. Spectra of the electrons emanated in a solid angle with an opening of 90° behind the target at the instant of simulation termination (t = 98 fs) in the irradiation of solid targets of thickness (*1*) 0.01 and (*2*) 0.02 μm, a low-density ($n_e = 5n_c$) 0.4-μm thick target (*3*), as well as a 0.02-μm thick target with a preplasma with a density which linearly varies from zero to the critical density over a length of (*4*) 4 and (*5*) 10 μm. Curve (*6*) represents the simulation spectrum of electrons accelerated from a 0.01 μm target with the inclusion of ionisation.

number and temperature of hot electrons. This growth of electron acceleration efficiency is related to the good channelling of the laser pulse during its propagation through the subcritical increasing-density plasma and efficient energy transfer of the laser beam to the energy of hot electrons accelerated behind its front. The latter is achieved, in particular, due to the development of plasma instabilities and stochastic electron heating in complex laser-plasma fields [12–15]. The electron generation efficiency would be expected to rise until the laser beam is completely depleted in the lengthy plasma corona.

3. Employment of accelerated electron beams for generating X-rays

The electron beams accelerated by a short laser pulse were used to generate X-ray radiation from the second target (converter target) placed immediately behind the laser target. To analyse the resultant X-ray radiation, the electrons accelerated in the laser target, whose parameters were calculated using the Mandor three-dimensional simulation code, were used as input data for the GEANT-4 code [16, 17]. The function of converter detector was fulfilled by a tantalum foil of thickness 16 μm to 8 mm. The choice of this converter is typical for obtaining hard X-ray and gamma-ray radiation, which is justified due to a sufficiently high radiation yield, low residual radioactivity, optimal physicomechanical properties, and simplicity of fabrication. The source of electrons incident on the converter target was assumed to be point-like; the energies and momenta of all electrons were transferred from the Mandor code. The simulations were made for three cases of laser-accelerated electron generation: with the use of a uniform solid laser target (with and without the inclusion of ionisation) and the preplasma target.

The outcome of our simulations was the radiation transmitted through the detector and the reflected radiation and their angular distributions. Furthermore, we simulated the transmitted and reflected electron fluxes. For a thick target, the main contribution to the secondary radiation spectrum is made by the bremsstrahlung rather than the characteristic radiation. This is clearly seen in Fig. 3, which shows the dependence of the secondary X-ray spectrum on the target thickness in the case when the electrons are accelerated in a 10-nm-thick solid target. The number of photons with energies above 300 keV is greatest for a converter target of thickness 800 μm. For X-ray radiation with energy ranging from tens of electronvolts to 300 keV it is advantageous to employ a 120-μm thick converter target. Thin targets (tens of micrometres in thickness) turn out to be most advantageous for generating individual monoenergetic characteristic lines.

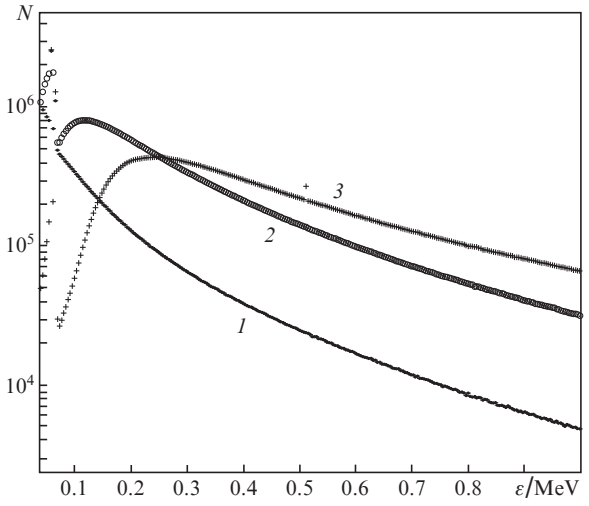

Figure 3. X-ray spectra from the converter target irradiated by the electrons, which are accelerated in a solid semitransparent tantalum laser target of thickness (*1*) 16.5, (*2*) 120, and (*3*) 800 μm.

Qualitatively, the same dependence is also typical for the electrons accelerated in preplasma targets. However, their use leads to the highest X-ray energy flux, as is seen in Fig. 4, which shows the X-ray spectra for electrons accelerated in different laser targets and the same converter target. In the tantalum target irradiation, the number of photons in the domain of the spectrum maximum (200–400 keV) is approxi-

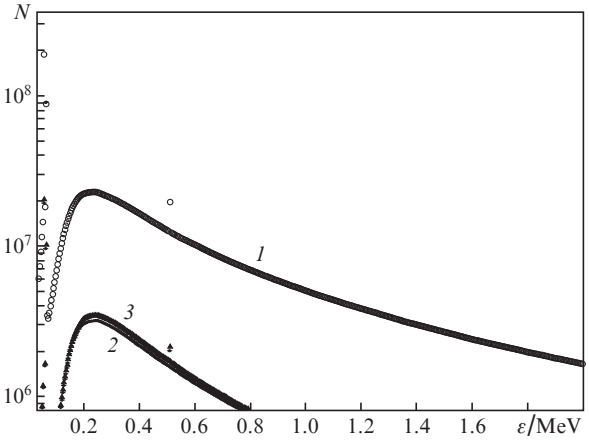

Figure 4. X-ray spectra of an 800-μm thick converter target irradiated by the electrons accelerated in (*1*) a preplasma laser target as well as in (*2*) a low-density target and (*3*) a solid target with the inclusion of ionisation.

mately six-to-seven times greater with the use of electrons accelerated in target with a 10-μm-long preplasma than with the electrons accelerated in low-density or solid laser targets. For the energetic tail of the spectrum (energies above 1 MeV) this difference may range up to several orders of magnitude.

The simulated X-ray radiation exhibits a slightly directional angular distribution. The X-ray energy flux is characterised by a higher directionality in the irradiation of the converter target by the electrons accelerated in solid and low-density targets. The directionality is also improved on lowering the thickness of converter target (Fig. 5). The angular width of the energy flux of secondary radiation increases with increasing thickness of the converter target as well as in the irradiation of the converter target by the electrons accelerated in a preplasma laser target. The resultant angular distribution is accounted for by the initial directionality of the electron beam accelerated in a laser target.

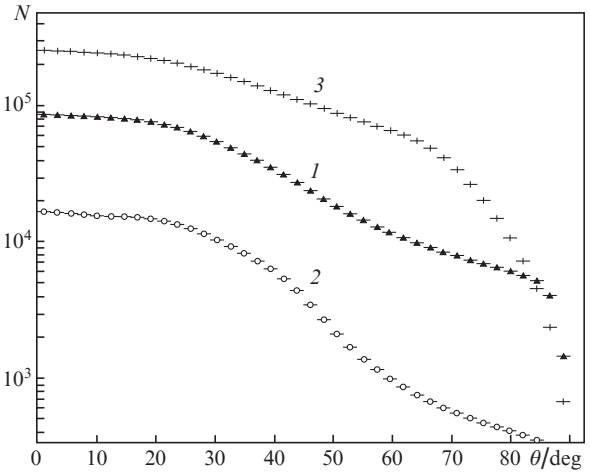

Figure 5. Angular distribution of the X-ray radiation for a converter target of thickness (*1*) 16.5, (*2*) 120, and (*3*) 800 μm irradiated by the electrons accelerated in a preplasma laser target.

4. Conclusions

The acceleration of electrons in different targets irradiated by a short (30-fs long) laser pulse with an energy of 300 mJ was studied by three-dimensional numerical simulations. It was shown that the use of low-density targets with an electron density $n_e \approx 5n_c$ or semitransparent solid foils, which are optimal for ion acceleration, does not maximise the temperature and number of particles in the generated electron beams. By contrast, targets with a plasma corona are advantageous to employ. It was found that the number and energy of the accelerated electrons emanated behind the target are determined by the dimension of target preplasma and increase with its thickness, i.e. the laser-to-hot electrons energy conversion coefficient increases, as does the hard X-ray radiation yield.

An important finding of our investigation is that going to a lengthy corona (10 μm) does not yet result in the saturation of this conversion coefficient and, hence, the optimal target for X-ray generation corresponds to an even longer corona. Moreover, although our preliminary simulations (less accurate) for preplasma dimensions of 20 and 30 μm showed some tendency for a lowering of the growth rate for the hot electron yield with increasing corona thickness, they did not correspond to the optimal preplasma dimension, which was supposedly longer than 30 μm. Three-dimensional simulations of electron acceleration in such a preplasma requires large computational resources and is our task for the nearest future. We emphasise that obviating this problem by way of two-dimensional simulations leads to fallacious results, because it provides an incorrect description of laser pulse propagation in subcritical plasmas [18]. In particular, because of erroneous description of the channelling of a laser pulse in two-dimensional simulations, its on-axis intensity may be several times lower in comparison with three-dimensional simulation data [19].

Therefore, our conclusion that the highest hard X-ray yield would be expected from targets with a lengthy plasma corona gives hope for the high efficiency of a layered target consisting of a low-density substance and a metal substrate. In this case, the preplasma might be produced and controlled by a low-intensity nanosecond prepulse. At present, there exists a technology for producing low-density (50–100 mg cm^{-3}) and highly homogeneous (with pore dimensions under 100 nm) films of nanocarbon tubes [20].

The characteristics of electron beams obtained in our three-dimensional simulations were used to analyse the secondary X-ray radiation from a converter target. The electrons accelerated by a short laser pulse with an energy of 300 mJ in a target with a 10-μm-thick preplasma were shown to generate 4×10^9 X-ray photons with energies ranging from 100 keV to 2 MeV in the irradiation of an 800-μm-thick tantalum target. The laser-to-hard X-ray energy conversion coefficient amounts to $\sim10^{-5}$, which is quite efficient for gamma-ray photons with energies of several hundred kiloelectronvolts.

Acknowledgements. This work was supported by the 'Extreme Laser Radiation: Physics And Fundamental Applications' Programme of the Presidium of the Russian Academy of Sciences and the Russian Foundation for Basic Research (Grant Nos 14-29- 09244-ofi-m, 15-02- 03042-a, and 16-02-00088-a), and its part dealing with low-density targets was supported by the Russian Science Foundation (Grant No. 14-12-00194).

References

1. Wenz J. et al. *Nat. Commun.*, **6**, 7568 (2015).
2. Serbanescu C.G. et al. *Rev. Sci. Instrum.*, **78**, 103502 (2007).
3. Toth R. et al. *Phys. Plasmas*, **14**, 053506 (2007).
4. Uryupina D.S., Ivanov K.A., Brantov A.V., et al. *Phys. Plasmas*, **19**, 013104 (2012).
5. Kutzner J., Witte H., Silies M., Haarlammert T., Huve J., Tsilimis G., Uschmann I., Forster E., Zacharias H. *Surf. Interface Anal.*, **38**, 1083 (2006).
6. Chen L.M. et al. *Phys. Rev. Lett.*, **104**, 215004 (2010).
7. Jiang S., Krygier A.G., Schumacher D.W., Akli K.U., Freeman R.R. *Eur. Phys. J. D*, **68**, 283 (2014).
8. Ivanov K.A., Brantov A.V., Kudryashov S.I., Makarov S.V., Gozhev D.A., Volkov R.V., Ionin A.A., Bychenkov V.Yu., Savel'ev A.B. *Laser Phys. Lett.*, **12**, 046005 (2015).
9. Brantov A.V., Govras E.A., Bychenkov V.Yu., Rozmus W. *Phys. Rev. Spec. Top. Accel. Beams*, **18**, 021301 (2015).
10. Landau L.D., Lifshitz E.M. *Electrodynamics of Continuous Media* (Oxford: Pergamon Press, 1960; Moscow: Nauka, 1982).
11. Romanov D.V., Bychenkov V.Yu., Rozmus W., Capjack C.E., Fedosejevs R. *Phys. Rev. Lett.*, **93**, 215004 (2004).
12. Ginzburg N.S., Zotova I.V., Kuritsyn A.V. *Zh. Tekh. Fiz.*, **69**, 3 (1999).
13. Sentoku Y., Bychenkov V.Yu., Flippo K., et al. *Appl. Phys. B*, **74**, 207 (2002).

14. Sheng Z.M., Mima K., Sentoku Y., Jovanović M.S., Taguchi T., Zhang J., Meyer-ter-Vehn J. *Phys. Rev. Lett*., **88**, 055004 (2002).
15. Bochkarev S.G., Brantov A.V., Bychenkov V.Yu., Torshin D.V., Kovalev V.F., Baidin G.V., Lykov V.A. *Fiz. Plazmy*, **40**, 365 (2014).
16. Agostinelli S., Allison J., Amako K., Apostolakis J., Araujo H., Arce P., Asai M., Axen D., Banerjee S., Barrand G., et al. *Nuclear Instrum. Methods Phys. Res., Sect. A*, **506**, 250 (2003).
17. Amako K., Guatelli S., Ivanchencko V., Maire M., Mascialino B., Murakami K., Pandola L., Parlati S., Pia M.G., Piergentili M., et al. *Nucl. Phys. B: Proc. Suppl.*, **150**, 44 (2006).
18. Pukhov A. *Rep. Prog. Phys.*, **66**, 47 (2003).
19. Pukhov A., Meyer-ter-Vehn J. *Phys. Rev. Lett*., **76**, 3975 (1999).
20. Fedotov P.V., Tonkikh A.A., Obraztsova E.A., Nasibulin A.G., Kauppinen E.I., Chuvilin A.L., Obraztsova E.D. *Phys. Status Solidi B*, **251**, 2466 (2014).